Corrosion Behaviour of Multiaxial Compressed AlMgSi Alloy

Abir Roy and Abhishek Kumar[*]

Department of Applied Mechanics, Motilal Nehru National Institute of Technology Allahabad, Prayagraj - 211 004, India
[*]E-mail: abhishek@mnnit.ac.in

ABSTRACT

In the present study, AlMgSi alloy was processed through multi-axial compression (MAC) to produce ultrafine-grained microstructure at room temperature. The AlMgSi alloys are widely used in automobile industries for making cylinder heads and brake disks etc. MAC was performed up to three cycles and showed improvement in mechanical properties. The impact of different strain levels upon microstructure changes is investigated using electron backscatter diffraction (EBSD). The average grain size reduced from an initial average grain size of ~ 124 to ~ 3 μm after completion of three cycles of MAC processing. Samples were tested for mechanical properties using uniaxial tensile test, hardness measurements, and corrosion. Tensile test results show a considerable increase in yield strength from ~90 MPa to ~249 MPa after 3 cycles of MAC. The average hardness value increased from 52 VHN to 90 VHN after 3 cycles of MAC. The corrosion resistance of MAC processed samples was found to decrease in comparison to solution-treated samples.

Keywords: Multiaxial compression; Potentiodynamic polarisation; Mechanical behaviour; AlMgSi alloy

1. INTRODUCTION

The severe plastic deformation (SPD) technique is a top-down approach to produce ultrafine-grained (UFG) materials from their bulk state and have improved mechanical characteristics such as ultimate tensile strength and hardness, which makes them more applicable for structural applications. Several SPD processes have been used to develop UFG materials, such as multi-axial compression (MAC)[1], accumulative roll bonding (ARB)[2], equal channel angular pressing (ECAP)[3], high-pressure torsion (HPT)[4] and constrained groove pressing (CGP)[5]. MAC is a repeated compression technique that develops large strains with relatively less loss of ductility in comparison to conventional deformation techniques. The moderate ductility in ultrafine-grained material processed by MAC is attributed to grain orientation randomisation[6,7]. MAC and multi-axial forging (MAF) are similar terms in use found in the literature[8]. MAC term is used to refer to the processing method employed in the present work. In the MAC processing, the same amount of strain is introduced in all the pressing directions, sequentially to a cuboidal-shaped sample kept in a constrained channel die set-up[9]. AlMgSi alloys are used in marine applications, therefore there is always a need for a material having higher strength with excellent corrosion resistance. Studies of corrosion behaviour of material processed by SPD methods are not yet well defined. Few corrosion studies on Al alloys indicated improvement in corrosion resistance after SPD, while some studies reported decreased corrosion resistance after SPD[10-12]. The irregularities of the corrosion behaviour primarily

depend on the corrosive solvents, the chemical composition of materials, and the type of deformation processes. According to literature MAC technique is less explored to produce ultrafine-grained materials; therefore, in the present work, an effort has been made to process AlMgSi alloy using MAC for the different magnitude of strain to understand the effect of MAC processing on the mechanical and corrosion behaviour.

2. RESEARCH METHODOLOGY

2.1 Materials

AlMgSi alloy was procured in square bars of cross-section 20 mm × 20 mm from the local market. The chemical composition of the procured alloy is given in Table 1.

Table 1. The chemical composition of procured AlMgSi alloy

Element	Mg	Si	Fe	Mn	Cu	Al
Composition (wt. %)	0.66	0.57	0.48	0.05	0.05	Bal.

The specimen of dimensions 40 mm × 20 mm × 20 mm were precisely cut for further processing. All samples were solution-treated at 530 °C for 2 h to acquire a homogenised microstructure[13]. The samples after solution-treatment have been stated as 'as-received'.

2.2 Material Processing

The as-received samples of AlMgSi alloy were processed as shown in Fig. 1 for multiple cycles of MAC. The lubricant Molybdenum disulfide (MoS_2) was used to reduce friction between the die and sample surface.
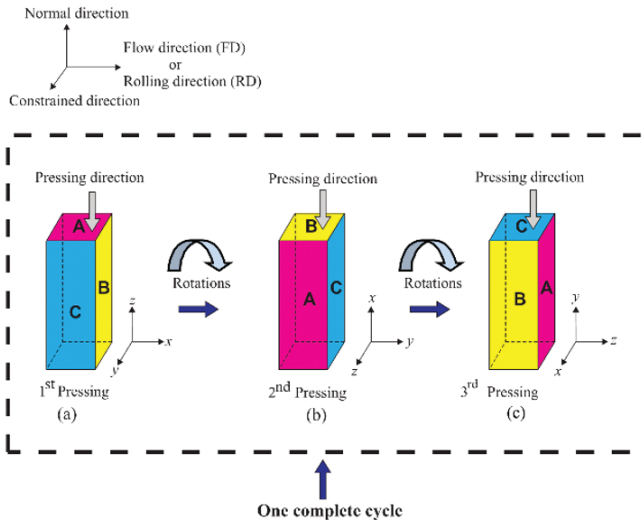
Figure 1. Schematic diagram of one complete cycle of MAC technique.

Because of the constrained flow of material in the die, the MAC process is considered similar to plane strain rolling conditions[14]. In the present study, a 50% reduction in the height of the specimen is achieved during the first pressing where the load is applied on face 'A' that resulted in material flow along face 'B' only as the face 'C' was constrained by the die channel walls. Two rotations of 90° were provided so that face B gets aligned with the loading direction, and again 50% reduction in length is achieved by compression. Similarly, the sample was pressed along face 'C'. The original geometry of the sample is restored after one complete cycle comprising of three orthogonal pressings as depicted in Figs. 1(a) to 1(c). The alloy was deformed up to three MAC cycles in the present work. The as-received sample is designated as A_0, and MAC processed samples are designated as $A_1, A_2,$ and $A_3,$ where the suffix represents the number of MAC cycles. In each pressing of MAC, the effective plastic strain (ε) imposed in the material can be calculated mathematically by using Eqn (1), as shown below[15,16]:

$$\varepsilon = \sqrt{\frac{2}{9}\left[\left(\varepsilon_{11} - \varepsilon_{22}\right)^2 + \left(\varepsilon_{22} - \varepsilon_{33}\right)^2 + \left(\varepsilon_{33} - \varepsilon_{11}\right)^2\right] + \frac{1}{3}\left(\gamma_{12}^2 + \gamma_{23}^2 + \gamma_{31}^2\right)}$$
(1)

where, ε_{11}, ε_{22}, and ε_{33} are uniaxial strains, and γ_{12}, γ_{23}, and γ_{31} denotes shear strain. The term $\varepsilon_{33} = 0$ and $\varepsilon_{11} = -\varepsilon_{22}$ due to plane strain deformation during MAC. Also, MAC comprises uniaxial compression therefore shear strain component $\gamma_{12} = \gamma_{23} = \gamma_{31} = 0$. The uniaxial strain for the present case for 50% reduction is calculated as

$$\left|\varepsilon_{11}\right| = \left|ln\left(\frac{h_f}{h_i}\right)\right| = \left|ln\left(\frac{20}{40}\right)\right| = 0.69,$$

where, h_i and h_f are the heights of samples, before and after compression respectively. Subsequently, the effective plastic strain expression given in Eqn (1) is simplified as:

$$\varepsilon = \sqrt{\frac{2}{9}\left[\left(2\varepsilon_{11}\right)^2 + \left(-\varepsilon_{11}\right)^2 + \left(-\varepsilon_{11}\right)^2\right]}$$

$$= \sqrt{\frac{12}{9}\left[\varepsilon_{11}^2\right]} \approx 0.8$$

After one complete cycle of MAC, the cumulative plastic strain introduced in the sample is 2.4 as calculated below using Eqn (2).

$$\varepsilon_{eff}^{one\ cycle} = N\sqrt{\frac{12}{9}\left[\varepsilon_{11}^2\right]}$$
(2)

$$= N\frac{2\sqrt{3}}{3}\left|\varepsilon_{11}\right| = N\frac{2\sqrt{3}}{3}\left|\ln\left(\frac{h_f}{h_i}\right)\right|$$

$$= 3 \times 0.8 = 2.40$$

where, N represents the number of pressings in one complete MAC cycle.

Samples were cut from mid-section perpendicular to normal direction (as shown in Fig. 1) for microstructure, hardness measurement, and corrosion studies. Al tensile samples were cut along the normal direction from the mid-section.

2.3 Orientation Imaging Microscopy

Orientation imaging microscopy (OIM) uses an electron backscattered diffraction (EBSD) pattern for analysing grains and grain boundaries based on the orientation of grains. EBSD measurements were done using a scanning electron microscope (Nova NanoSEM 450). The EBSD scan area considered for the study was $400 \times 400\ \mu m^2$ with a step size of 0.2 μm. EBSD testing samples were mirror-polished using emery paper and alumina paste. Additionally, samples were electro-polished on Struers' LectroPol-5 at 13 V for 17 s with an electrolyte containing 78 ml perchloric acid, 90 ml distilled water, 730 ml ethanol, and 100 ml butoxyethanol.

2.4 Mechanical Testing

Microhardness testing was done using the BAREISS Digi-test machine. A minimum of 10 indents was made by applying 50 g load with a dwell time of 10 s for hardness measurement.

The tension test was utilised to measure the yield strength, ultimate tensile strength, and percentage elongation of AlMgSi Alloy. The tension test specimens were made from the various processed samples using a wire-cut EDM machine to get the final size as per ASTM-E8. Tensile specimens were tested with a 12 mm gauge length and a 3 mm thickness using Tinius Olsen Benchtop mechanical testing system.

A constant strain rate of 2 mm/min was used throughout for standard tensile tests at room temperature. The tests were repeated three times on each sample and the mean values are reported.

2.5 Electrochemical Characterisation

Potentiodynamic polarisation testing was carried out on as-received and deformed samples. The exposed area was taken nearly as 1 cm². Polarisation measurements and electrochemical impedance spectroscopy (EIS) were conducted on the AutoLab PGSTAT302N potentiostat system. A three-electrode cell was used to measure EIS data at room temperature. The specimen, which acts as the working electrode, was dipped in 3.5 wt%

NaCl aqueous solution with pH = 6, with a saturated calomel electrode (SCE) and a platinum mesh as the reference and counter electrode, respectively. All samples were immersed in the electrolyte for 60 min. for stabilising the open circuit potential. A scan rate of 0.2 mV/s and scanning potential in the forward direction from −1500 mV to 1500 mV was used to obtain the potentiodynamic polarisation curves. The obtained electrochemical data was analysed using Nova 1.11 software.

Corrosion current (i_{corr}) and corrosion potential (E_{corr}) for polarisation curves can be calculated by the Tafel extrapolation method. Corrosion current helps in predicting the Corrosion rate with the help of following Eqn (3)[17].

$$CR = \frac{0.00327\ I_{corr}\ EW}{\rho A} \tag{3}$$

where, CR = corrosion rate in mm/year, I_{corr} = corrosion current in μA, EW = equivalent weight in grams, A = contact area in cm^2 and ρ = density in g/cm^3.

3. RESULTS AND DISCUSSION

3.1 Electron Backscatter Diffraction

Figure 2 shows band contrast maps found from OIM measurements. In OIM measurements, the highly strained regions are not indexed properly, and it returns a black pixel (black regions) in the maps. From Fig. 2, it is concluded that the sample A_0 consists of coarse grains and as the number of MAC cycles increases there is more reduction in grain size in comparison to the as-received sample, A_0.

Grain diameter was calculated using EBSD post-processing software, HKL Channel 5. The area fraction method was used to measure average grain size because of the presence of non-uniform grains in microstructure[18].

Figure 3 shows the average grain size of MAC processed samples. The average grain size of the A_0, A_1, A_2, and A_3 sample were estimated as ~124 µm, ~21 µm, 5 µm, and ~3 µm,
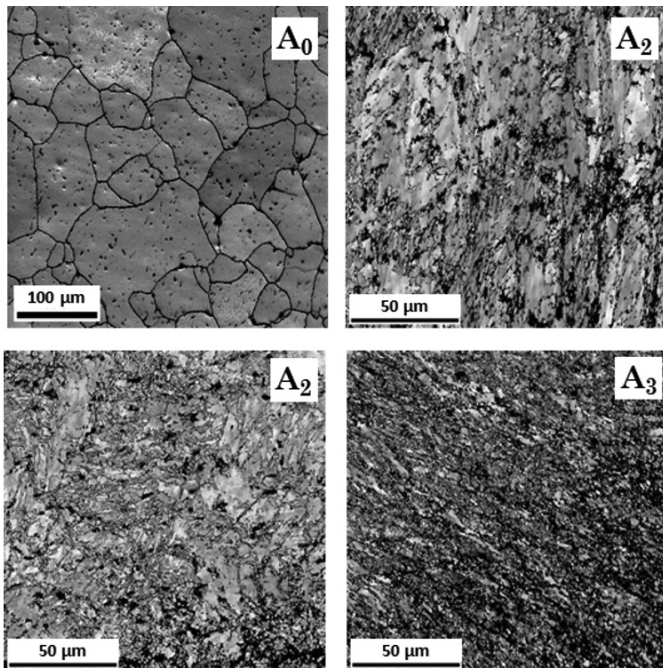
Figure 2. Band contrast maps A_0, A_1, A_2, and A_3 samples.
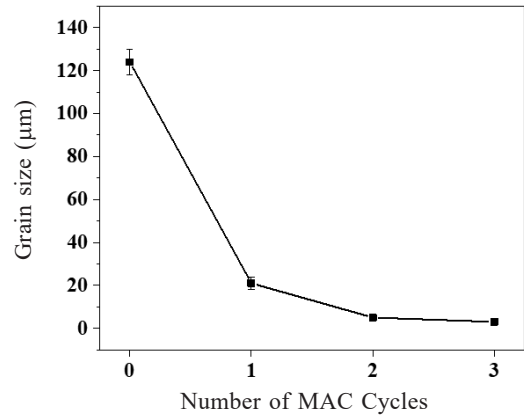
Figure 3. Variation of grain size with the number of MAC cycles.

respectively. The maximum amount of grain size reduction was observed in the first MAC cycle, in comparison to the second and third MAC cycles.

3.2 Mechanical Properties

Deformation through MAC leads to straining of the samples that in turn affects the microhardness properties. Figure 4 shows the variation of microhardness with MAC cycles. Figure 4 shows an increase in average hardness value from 52 VHN to 90 VHN after 3 cycles of MAC. This increment in hardness values is ascribed to the strain hardening phenomenon. Due to the straining of the material, dislocation density within the material increases due to which mutual interaction of dislocations within grains increases. This mutual interaction results in the blocking of dislocation motion by the presence of subgrain boundaries[19]. From the hardness results, it can be concluded that there is a continuous increment of hardness values, and at a higher number of cycles, this rate of increase is lower in comparison to the rate of increment at lower cycles which are also reported in the literature on SPD processes[20,21].

Figure 5 shows an increase in tensile strength with an increase in cumulative strain values in the samples. However, due to the accumulation of strain, the materials become brittle at higher cycles which leads to a decrement of percentage
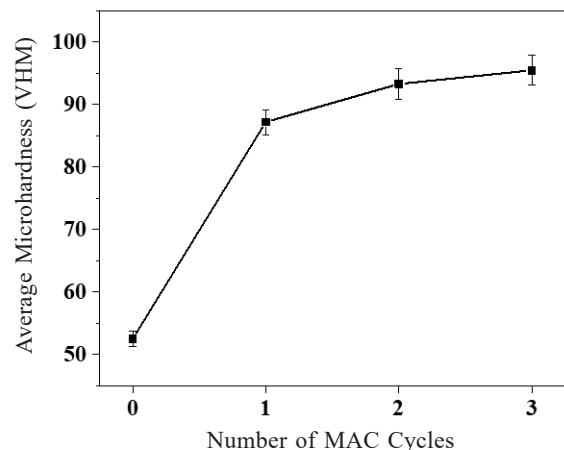
Figure 4. Variation in average microhardness value for A_0, A_1, A_2, and A_3 samples.
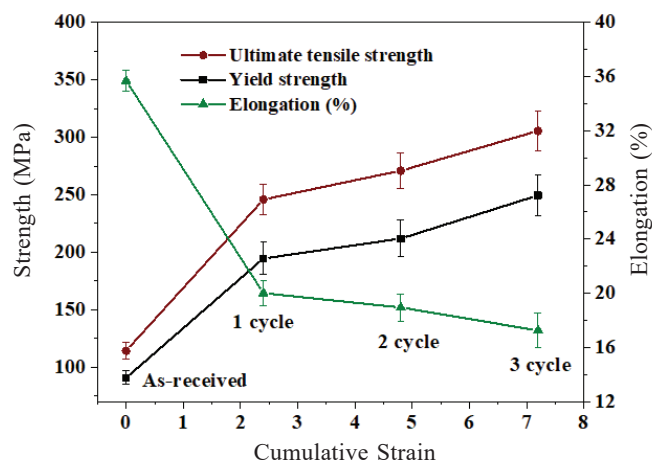
Figure 5. Variation of UTS, YS, and percentage elongation with cumulative strain.

Figure 6. Potentiodynamic polarisation curves of as-received and MACed AlMgSi alloy.

elongation values. Percentage elongation decreased from ~35% for the A_0 sample to ~17% for the A_3 sample. SPD processed materials show low ductility with high strength[22]. The Yield strength (YS) increases from 90 MPa for the A_0 sample to 249 MPa for the A_3 sample. Similarly, the ultimate tensile strength (UTS) was found to increase from 122 MPa for the A_0 sample to 308 MPa for the A_3 sample.

During MAC processing, a high amount of strains are imparted in the material, due to which grain size reduces, and thus increasing the tensile strength of the materials as explained by Hall–Petch relationship[23]. The increase in tensile strength properties after MAC processing is attributed to grain refinement and strain hardening mechanisms.

3.3 Electrochemical Results

Figure 6 shows potentiodynamic polarisation curves of A_0, A_1, A_2, and A_3 samples. The corrosion rate was calculated using TAFEL extrapolation. The two polarisation curves intersect at a point where the material starts corroding. The corresponding potential is called corrosion potential (E_{corr}) and the corresponding current is corrosion current (i_{corr}). This value of the corrosion current is used to calculate corrosion rates. Formation of a more noble (better corrosion resistant) surface is achieved if there is a shift of E_{corr} value with time in the positive direction and also decreasing corrosion current (i_{corr}) leads to a lower corrosion rate[24]. Tafel slopes β_a, β_c, E_{corr}, i_{corr}, and corrosion rate values of different sample conditions have been summarised in Table 2.

Table 2 clearly shows an increase in corrosion rate as the strain increases in the material. Corrosion occurs due to the formation of local galvanic cells. In AlMgSi alloy, the α-AlFeSi phase particles act as cathodes and aluminium matrix as an anode. This α-AlFeSi phase helps in activating the anodic dissolution of the surrounding aluminium matrix by the reduction of oxygen. MAC cycles lead to reduction, which resulted in the increment of local galvanic cells. Thus, the increase of corrosion rate with the increase in the number of MAC cycles can be attributed to the enhanced dissolution of the matrix[25]. A comparison of the present work with other processing techniques on similar materials has been presented in Table 3. The results show improved mechanical characteristics as compared to reported in the literature.

Table 3. Comparison of mechanical properties of AlMgSi alloys processed by different processing routes

Processing method (Material)	YTS (MPa)	UTS (MPa)	Hardness (Hv)	Reference
CR* (AlMgSi)	223	248	85.5	[26]
ACR# (Al6061)	247	–	71.5	[27]
ARB$ (Al6061)	–	363	85	[28]
ECAP! (AA6060)	344	355	120	[29]
MAC (AlMgSi)	249	308	95	Present work

*CR-cryorolling, #ACR-asymmetric cryorolling, $ARB-accumulative roll bonding, and !ECAP-equal channel angular pressing.

4. CONCLUSIONS

The multi-axial compression process was successfully applied on AlMgSi alloy for up to three cycles. The averaged grain size values reduced from ~124 μm for the A_0 sample to ~3 μm for the A_3 sample. Enhancement of average hardness values by ~82% was achieved through MAC processing. Similarly, yield strength and ultimate tensile strength considerably improved by ~176% and ~152%, respectively. This improvement in mechanical properties is attributed to strain hardening and grain refinement. For AlMgSi alloy, the corrosion rate increased from 8.357×10^{-3} mm/year for the as-received sample to 17.436×10^{-3} mm/year for the

Table 2. Electrochemical parameters obtained from potentiodynamic polarisation test for as-received and MACed AlMgSi alloy

No. of Pass	E_{corr} (mV)	β_a (mV)	β_c (mV)	i_{corr} (μA/cm²)	Corrosion rate (mm/year)
A_0	−733.326	68.2	105.1	0.767	8.357×10^{-3}
A_1	−738.435	75.4	119.8	1.154	12.572×10^{-3}
A_2	−745.887	77.3	135.2	1.443	15.720×10^{-3}
A_3	−752.386	78.4	158.4	1.601	17.436×10^{-3}

3rd cycle sample. This trend can be understood by the enhanced dissolution of the matrix due to increases in local galvanic cells formed by grain reduction that resulted from MAC processing.

REFERENCES

1. Ghosh, A.K. Method for Producing a Fine Grain Aluminum Alloy Using Three Axes Deformation. 26 January 1988, U.S. Patent No. 4721537.

2. Saito, Y.; Utsunomiya, H.; Tsuji, N. & Sakai, T. Novel ultra-high straining process for bulk materials-development of the accumulative roll-bonding (ARB) process. *Acta Mater*., 1999, **47**(2), 579−583.
    doi: 10.1016/S1359-6454(98)00365-6

3. Valiev, R.Z. & Langdon, T.G. Principles of equal-channel angular pressing as a processing tool for grain refinement. *Prog. Mater. Sci*., 2006, **51**(7), 881−981.
    doi: 10.1016/j.pmatsci.2006.02.003

4. Zhilyaev, A.P. & Langdon, T.G. Using high-pressure torsion for metal processing: Fundamentals and applications. *Prog. Mater. Sci*., 2008, **53**(6), 893−979.
    doi: 10.1016/j.pmatsci.2008.03.002

5. Singh, R.; Singh, D.; Sachan, D.; Yadav S.D. & Kumar A., Microstructural Evolution and Mechanical Properties of Constrained Groove-Pressed 304 Austenitic Stainless Steel. *J. Mater. Eng. Perform.,*2021.
    doi: 10.1007/s11665-020-05372-x

6. Biswas, S. & Suwas, S. Evolution of sub-micron grain size and weak texture in magnesium alloy Mg–3Al–0.4Mn by a modified multi-axial forging process. *Scr. Mater*., 2012, **66**(2), 89−92.
    doi: 10.1016/j.scriptamat.2011.10.008

7. Sabat,R.K.; Mishra, R.K.; Sachdev,A.K. & Suwas,S. The deciding role of texture on ductility in a Ce containing Mg alloy, *Mater. Lett.*, 2015, **153**, 158−161.
    doi: 10.1016/j.matlet.2015.03.036

8. Cherukuri, B. & Srinivasan, R. Properties of AA6061 Processed by Multi-Axial Compressions/Forging (MAC/F). *Mater. Manuf. Process*., 2006, **21**(5), 519−525.
    doi: 10.1080/10426910500471649

9. Gurao, N.P.; Kumar, P.; Sarkar, A.; Brokmeier, H.G. & Suwas, S. Simulation of deformation texture evolution during multi axial forging of interstitial free steel. *J. Mater. Eng. Perform.*, 2013, **22**(4), 1004−1009.
    doi: 10.1007/s11665-012-0388-8

10. Wei, W.; Wei, K.X.; & Du, Q.B. Corrosion and tensile behaviors of ultra-fine grained Al-Mn alloy produced by accumulative roll bonding, *Mater. Sci. Eng. A*, 2007, **454**, 536-541.
    doi: 10.1016/j.msea.2006.11.063

11. Hockauf, M.; Meyer, L.W.; Nickel, D.; Alisch, G.; Lampke, T.; Wielage, B.; & Kruger, L. Mechanical properties and corrosion behaviour of ultrafine-grained AA6082 produced by equal-channel angular pressing*, J. Mater. Sci.*, 2008, **43**, 7409-7417.
    doi: 10.1007/s10853-008-2724-9

12. Naeini, M.F.; Shariat, M.H. & Eizadjou, K. On the chloride-induced pitting of ultra fine grains 5052 aluminum alloy produced by accumulative roll bonding process. *J. Alloy. Comp*., 2011, **509**, 4696-4700.
    doi: 10.1016/j.jallcom.2011.01.066

13. Nurislamova, G.; Sauvage, X.; Murashkin, M.; Islamgaliev, R. & Valiev, R. Nanostructure and related mechanical properties of an Al-Mg-Si alloy processed by severe plastic deformation. *Philos. Mag. Lett.*, 2008, **88**(6), 459-466.
    doi: 10.1080/09500830802186938

14. Roy A.; Tiwari M.; Sahu,S.; Mishra, S. & Kumar, A. Microstructure, texture and mechanical properties of Al-Mg-Si alloy processed by multiaxial compression. *J. Mater. Eng. Perform*., 2020, **29**(6), 3876–3888.
    doi: 10.1007/s11665-020-04917-4

15. Xia, X.S.; Huang, J.; Zhang, R.C.; Zhao, Q.; Hu, Q.H.; Deng, T.Q.; Xiao, Y.L. & Sun, C.J. Evolution of microstructure and mechanical properties of AZ61 Mg alloy during cyclic closed die forging. *Mater. Res. Innov*., 2013, **17**(1), 130−134.
    doi: 10.1179/1432891713Z.000000000203

16. Kumar, S.S.S. & Raghu, T. Bulk processing of fine grained OFHC copper by cyclic channel die compression. *Int. J. Mater. Res*., 2015, **106**(12), 1230−1239.
    doi: 10.3139/146.111302

17. Verma, N.; Singh, S., Rao, P.N.; Jayaganathan, R.; Midathada, A.; Verma, K. & Ravella, U.K. Elevated corrosion in strain hardened Al Mg alloy. *Vacuum*, 2018, **157**, 402−413.
    doi: 10.1016/j.vacuum.2018.09.010

18. Suwas, S. & Ray, R.K. Crystallographic texture of materials, engineering materials and processes. *Springer-Verlag London*, 2014, pp 256.
    doi: 10.1007/978-1-4471-6314-5

19. Ito, Y. & Horita, Z. Microstructural evolution in pure aluminum processed by high-pressure torsion. *Mater. Sci. Eng. A*., 2009, **503**, 32–36.
    doi: 10.1016/j.msea.2008.03.055

20. Xing, Z.P.; Kang, S.B. & Kim, H.W. Structure and properties of AA3003 alloy produced by accumulative roll bonding process. *J. Mater. Sci.,* 2002, **37**(4), 717−722.

21. Nakashima, K.; Horita, Z.; Nemoto, M. & Langdon, T.G. Development of a multi-pass facility for equal-channel angular pressing to high total strains. *Mater. Sci. Eng. A*., 2000, **281**(1), 82−87.
    doi: 10.1016/S0921-5093(99)00744-3

22. Yadav, P.C.; Sinhal, A.; Sahu, S.; Roy, A. & Shekhar, S. Microstructural inhomogeneity in constrained groove pressed Cu-Zn alloy sheet. *J. Mater. Eng. Perform*., 2016, **25**(7), 2604–2614.
    doi: 10.1007/s11665-016-2142-0

23. Huang, X.; Kamikawa, N.; & Hansen, N. Strengthening Mechanisms in Nanostructured Aluminum. *Mater. Sci. Eng. A*, 2008, **483**, 102–104.
    doi: 10.1016/j.msea.2006.10.173

24. Vayenas, C.G.; White, R.E. & Gamboa-Aldeco, M. E. Modern aspects of electrochemistry No. 42. *Springer,* New York, 2008, p 194.

doi: 10.1007/978-0-387-49489-0

25. Korchef, A. & Kahoul, A. Corrosion behavior of commercial aluminum alloy processed by equal channel angular pressing. *Int. J. Corros*, 2013, **2013**(1), 1-11.
doi: 10.1155/2013/983261

26. Panigrahi, S.K. & Jayaganthan R. A study on the mechanical properties of cryorolled Al–Mg–Si alloy. *Mater. Sci. Eng. A*.2008, **480**, 299–305.
doi: 10.1016/j.msea.2007.07.024

27. Yu, H.; Tieu, K.; Lu, C.; Liu, X.; Godbole, A. & Kong, C. Mechanical properties of Al–Mg–Si alloy sheets produced using asymmetric cryorolling and ageing treatment. *Mater. Sci. Eng. A.*, 2013, **568**, 212–218.
doi: 10.1016/j.msea.2013.01.048

28. Lee, S.H.; Saito, Y.; Sakai, T.& Utsunomiya, H. Microstructures and mechanical properties of 6061 aluminum alloy processed by accumulative roll-bonding. *Mater. Sci. Eng. A.*. 2002, **325**, 228-235.
doi: 10.1016/S0921-5093(01)01416-2

29. Khelfa, T.; Rekik, M.; Muñoz, J.; Cabrera, J. & Khitouni, M. Microstructure and strengthening mechanisms in an Al-Mg-Si alloy processed by equal channel angular pressing (ECAP). *Int. J. Adv. Manuf. Technol.*, 2018, **95,** 1165–1177.
doi: 10.1007/s00170-017-1310-1

CONTRIBUTORS

Mr Abir Roy received his BTech in Mechanical Engineering from Chhatrapati Shahu Ji Maharaj University, Kanpur, and MTech in Materials Science and Engineering from MNNIT Allahabad. He is currently pursuing his PhD from the Department of Applied Mechanics, MNNIT Allahabad.
He has performed experimental work and analysis of results in the current study.

Dr Abhishek Kumar is an Associate Professor in the Department of Applied Mechanics, MNNIT Allahabad. He has teaching and research experience of more than 16 years. His current research interests include severe plastic deformation, texture, and corrosion analysis of Al-alloys and the mechanical behaviour of dispersed polymers.
The present work was carried out under his supervision.